Experimental and Computational Investigation of Valve Motion in a Resonant Pulse Combustor

Daniel E. Paxson[1], H. Douglas Perkins[2]
NASA Glenn Research Center, Cleveland, Ohio, 44135

Shaye Yungster[3]
HX5, LLC, NASA Glenn Research Center, Cleveland, Ohio, 44142

The motion of a passive reed-type valve and a poppet-style valve operating in a small scale, liquid-fueled pulse combustor is investigated experimentally. Valve position and combustion chamber pressure are simultaneously measured using an in-house fabricated optical position probe. The reed valve configuration is found to operate in a self-aspirated mode, generating significant pressure gain. The poppet valve configuration cannot operate without forced air, and does not generate pressure gain. Both type valves are tested in combustors of multiple lengths. Close examination of the respective valve motions indicate that the reed valve is highly non-linear, with unique attributes that appear essential for self-aspiration. Dynamic models for the motion of each valve are implemented in a computational fluid dynamic (CFD) simulation of the pulse combustor in order to assess if this unique valve motion is critical to successful operation. The results show that it is. The implications of these results are discussed. The need for active actuation with feedback control, rather than passive valve actuation is highlighted as a critical technology for practical resonant pulse combustors.

Nomenclature

A_{ch}	=	inlet channel cross sectional area, in^2
A_p	=	poppet valve area, in^2
A_{vr}	=	reed valve open area, in^2
A_{vs}	=	slider valve open area, in^2
d_{ch}	=	inlet channel diameter, in
δ	=	air gap between valve and valve seat, in
f	=	valve friction coefficient, $lb_f \cdot s/in$
F_s	=	spring force, lb_f
g_c	=	Newton constant, $lb_m \cdot ft/ lb_f \cdot s^2$
k	=	spring constant, lb_f/in
L	=	tailpipe length, in.
m	=	valve mass, lb_m
p_a	=	ambient pressure, psia
p_{cc}	=	combustion chamber pressure, psia
R_{closed}	=	radius corresponding to the slider valve closed position, in
R_{open}	=	radius corresponding to the slider valve fully open position, in
R_{vs}	=	radius corresponding to the slider valve tip, in

[1] Aerospace Research Engineer, Research and Engineering Directorate, AIAA Associate Fellow
[2] Aerospace Research Engineer, Research and Engineering Directorate, AIAA Senior Member
[3] Aerospace Research Engineer, Research and Engineering Directorate, AIAA Senior Member

t = time, sec
T = temperature, R
T_0 = reference temperature, 540 R
v_v = valve linear velocity, in/s
V_{fiber} = fiber optic probe voltage, V
x_v = valve linear position, in

I. Introduction

Resonant Pulse Combustors (RPC) represent one of the least investigated approaches to pressure gain combustion (PGC) since interest in the concept re-emerged in the 21st century. This is surprising since, to date, they are the only implementation of PGC that has demonstrated unequivocal pressure gain (e.g., a total pressure rise across the combustor, or self-aspirated static operation in the open atmosphere) [1-3]. Additionally, when they are combined with ejector technology, they generate pressure gain at overall air/fuel equivalence ratios that are compatible with their use in gas turbines [4, 5]. Furthermore, detailed computational fluid dynamic (CFD) simulations have indicated that the so-called Ejector Enhanced Resonant Pulsed Combustor (EERPC) configuration can work well at the high pressures and temperatures associated with modern gas turbines, while simultaneously producing competitively low emissions [6]. The thermodynamic benefits of EERPC pressure gain are substantial in terms of reduced specific fuel consumption (and associated greenhouse gas reduction) [5]. The demonstrated capability to operate with liquid or gaseous fuels also makes it attractive for use in the gas turbine environment.

One vexing challenge that high-performance pulse combustors present however, is the requirement of a mechanical inlet air valve. A greatly simplified pulse combustion cycle is illustrated in Fig. 1 [7]. Air enters the combustion chamber through the open valve. It is mixed with fuel, ignited, and undergoes a confined combustion process. Confinement is provided on the left by the inlet valve, which closes as the pressure rises in the chamber. It is provided on the right by the fluid in the tailpipe and its associated inertia. Combustion produces a rapid rise in the chamber pressure. This propagates a compression wave down the tailpipe and accelerates the fluid therein. The accelerated fluid rapidly exits the tailpipe allowing expansion of the combustion chamber products. Due to the combined expansion process (aka, blowdown) and reflection of gasdynamic waves from the open end of the tailpipe, the chamber pressure eventually drops below the ambient pressure. As a result, the inlet valve opens and allows a new charge of air and fuel to enter. The low chamber pressure also decelerates the exiting tailpipe fluid to such a degree that it briefly reverses direction. The reversed hot combustion products ignite the fresh charge, and the cycle begins anew. A more detailed illustration of the cycle may be found in [6]. Therein it is shown that there is a complex combination of acoustic, Helmholtz, mixing, chemical kinetic, coherent vortex, evaporative, and mechanical time scales that must synchronize for successful resonant operation. The overall operational frequency of this process depends on many factors, but it is dominated by the combined combustion chamber and tailpipe length. For pulse

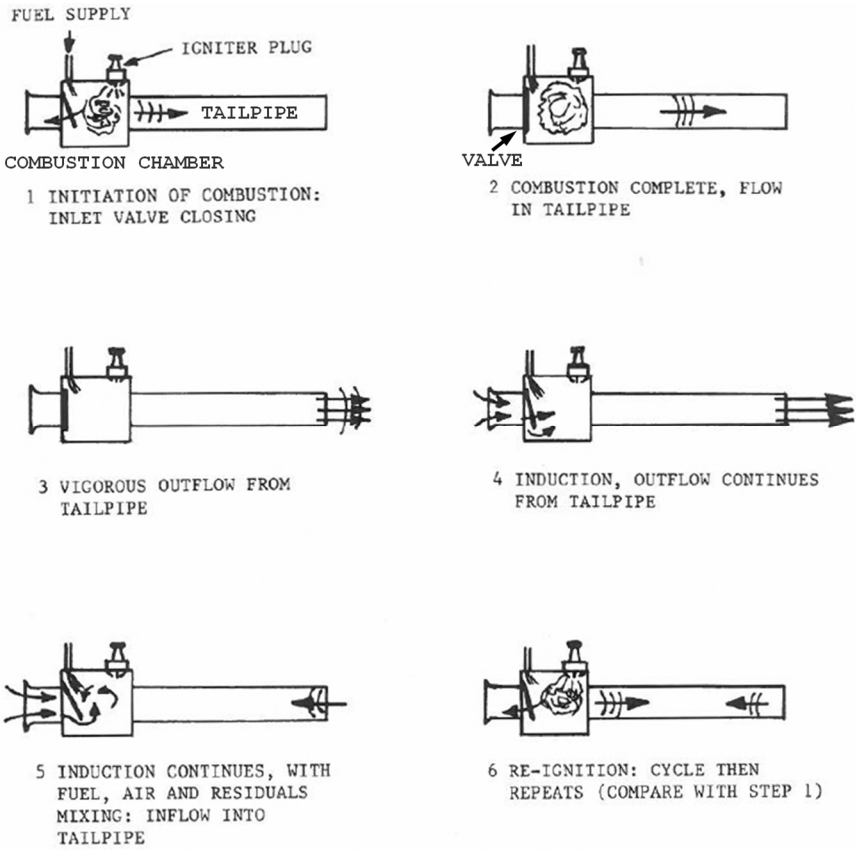

Fig. 1 Schematic of pulse combustor cycle [7]

combustors that are appropriate for gas turbine applications, this implies operation at several hundred hertz. The chamber pressure during operation typically oscillates from approximately twice to one half of the ambient (or compressor discharge) pressure. Designing an air valve that can simultaneously operate at these frequencies, sustain the harsh combustor pressure and temperature environment, and fit within the geometric constraints of the combustor is challenging. Furthermore, the particular motion of the valve required for high performance operation is complex [8, 9].

Many high frequency pulse combustors utilize a passive (i.e., actuated by internal fluid and mechanical forces), reed-type inlet valve similar to that shown schematically in Fig. 2. The design was originated by the Curtis Dyna-Fog Company in approximately 1950. Although the valve delivers the requisite motion, it does not last long. The harsh thermal environment, significant flexure on opening, and subsequent rapid deceleration (i.e., slamming) on closing can result in valve failure after only minutes of cumulative run time. An example of a failed reed valve is shown in

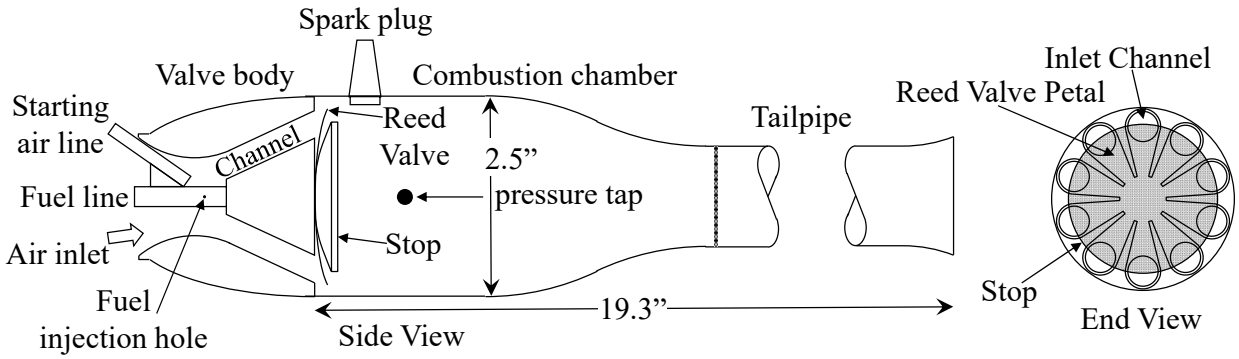

Fig. 2 Side and end view of a typical passive, high-frequency, reed valve. The reed valve is shown partially open but is closed at rest.

Fig.3 [5].

Robust, active valves (i.e., externally actuated) with exceptionally long lifetimes have been fabricated and tested [2]. Unfortunately, their performance is below that of the original reed valve in terms of pressure gain. The reason for this is likely that their motion (e.g., duty cycle, slew rate, phase angle, etc.) is not quite matched to the other time scales. Furthermore, the active designs to date do not generally have independently variable parameters.

The present work began as an effort to develop a new and improved passive valve design that would deliver the requisite motion, but last longer than the original reed valve. If successful, this valve would enable laboratory studies of high-pressure, high-temperature operation relevant to in-situ gas turbine operation.

Unfortunately, the new valve did not yield successful, self-sustained, self-aspirated operation when tested. However, the diagnostic effort to determine why it didn’t work, and why the reed valve works so well is of value to report. It serves as a guide for future passive designs, and as well, to highlight the requirements for future high-performance active designs, including those with feedback control.

The new valve design, heretofore called the poppet, will first be described and compared to the original reed valve. This will be followed by a description of the diagnostic equipment and test environment. Results of testing for both the original reed valve and the new poppet valve, which share a common valve head, inlet, combustion chamber, and tailpipe, will be presented and discussed. Simple mathematical models of the two valves are then implemented in a validated, axis-symmetric, computational fluid dynamic (CFD) simulation of the pulse combustor and compared to the experimental measurements. The results confirm the conclusion that passive mechanical valves for high-frequency pulse combustors require specific motion beyond just high frequency to achieve operational success. Similarly, it is concluded that active valve designs will require considerable flexibility in their motion capability in order to yield high-performance operation.

Fig. 3 Failed spring-steel reed valve

II. Experimental Setup

A. New Air Valve Design

The passive, poppet valve concept is shown in Fig. 4. The flow path and internal dimensions of the valve head are identical to those for the reed valve. In fact, the original reed valve and stop can be and were used with this valve head with only a slight change in performance due to the poppet sleeve which creates some minor blockage in the inlet passage. In place of the spring steel reed petals, the new valve has 10 titanium poppet valves, each with a spring and damper system external to the combustor. The damper is stiff synthetic material. Since the valve stop is on the outside of combustor, there is no need for an internal stop. However a similarly shaped piece was fabricated to serve as a diverter and directed the flow toward the outer radius of the combustion chamber. The total weight of the 10 poppet valves, springs, dampers and stops is approximately the same 0.0042 lb_m as the original reed valve. The maximum linear travel of the poppet is approximately half that of the reed valve, as shown in Fig. 5. Nevertheless, when the poppet is fully open, the open area, defined as the product of the valve circumference and the gap, δ, is equal to the inlet channel area (see Fig. 2). The short travel, the poppet material, and the spring location outside of the hot combustion chamber were all features of the long-life design. The short travel also resulted in a lighter poppet, which improved frequency response.

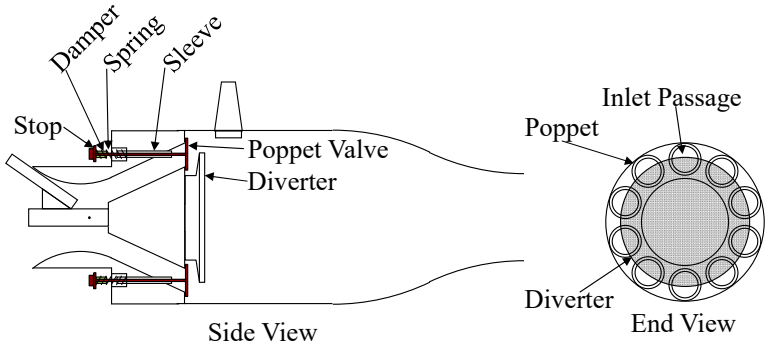

Fig. 4 Side and end view of the passive, high-frequency, poppet valve

B. Diagnostic: Valve Position Probe

In order to measure the valve motion, a novel optical valve position probe was fabricated and installed. It is based on a prototype described in [9]. The probe utilizes two optical fibers housed in a metal sheath. An infrared LED (950 nm wavelength) transmits down one fiber, reflects from the valve, and is received by an infrared phototransistor (in an appropriate amplification circuit) through the second fiber. The installed arrangement is shown schematically in Fig. 6 for the two valve types. The simple principle of operation is that the more the valve is open (i.e., the further it is from the probe tip where light is emitted), the less light will be reflected from the valve and detected by the phototransistor. The system was tested under a number of dynamic, uninstalled scenarios where the poppet or reed valve could be vibrated at known or natural frequencies. It performed well and demonstrated excellent frequency response well above 50 kHz..

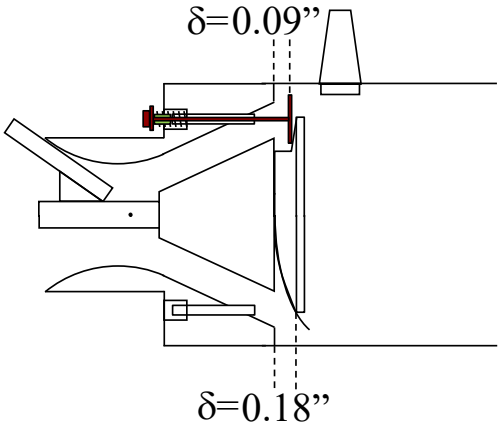

Fig. 5 Comparison of fully extended poppet (top) and reed valve (bottom) frequency, poppet valve

The only major shortcoming identified to date is that the probe can’t be calibrated in the present setting. The 950 nm light on which it is based was selected because it reflects well from most surfaces. However, it is sensitive to high temperatures. Any calibration of position versus signal done under ambient conditions is not meaningful during pulse combustor operations where the device gets very hot, very quickly. For this work however, knowing the exact valve position is not as critical as knowing when it is opening, closing, and shut, relative to the chamber pressure with which it is forced. All of the results presented were therefore digitally high-pass filtered after acquisition with a cut-off frequency of 60 Hz. Filtering was performed in both the forward and reverse directions to remove any phase shift. Two minor shortcomings of the sensor are relevant to note as well. First, any rotation of the poppet valve or twisting of the reed valve cannot be distinguished from linear motion. Second, the sensor is highly non-linear. The change in voltage per unit of movement is much larger when the valve is near the fully closed position than when it is near the fully open position.

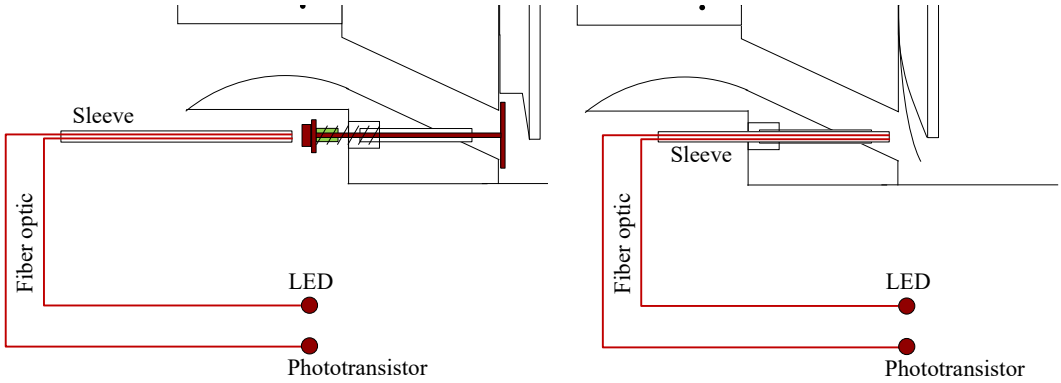

Fig. 6 Schematic of the dynamic valve position sensor installed in the poppet (left) and reed (right) valves.

C. Additional Instrumentation, Installation, and Operation

Photographs of the installed pulse combustor are shown in Fig. 7. Figure 7a shows a high-frequency Kulite absolute pressure transducer mounted in a 2.5 in. long standoff tube. It is used to measure combustion chamber

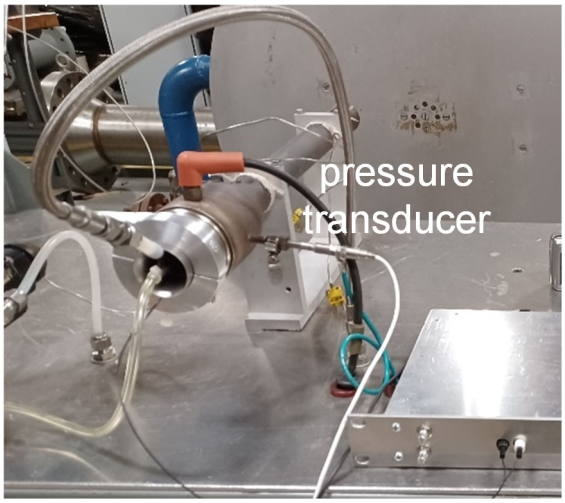

(a)

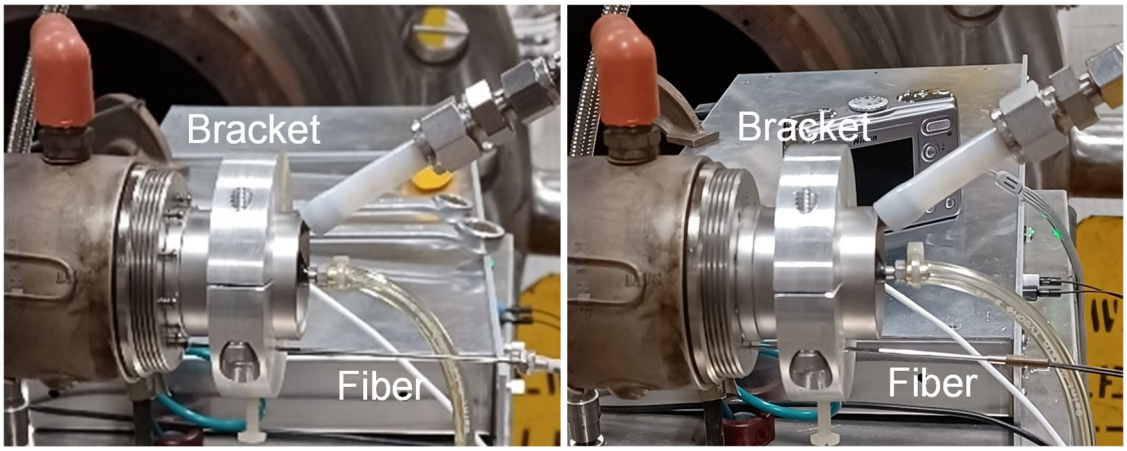

(b) **(c)**

Fig. 7 Installed pulse combustor with pressure transducer visible (a); fiber optic sensor in poppet valve configuration (b); fiber optic sensor in reed valve configuration (c)

pressure. During limit cycle operation the time-averaged value of this pressure relative to the ambient pressure correlates well to thrust measurements [1] and is thus a figure of merit for performance. Figures 7b and 7c show the fiber optic position sensor installed in the poppet and reed valve configurations respectively. Not shown in the figure is an external microphone which measures the acoustic signal emitted by the combustor. The microphone signal was used to identify operating frequency and as a crude measure of performance for the limited testing (described later) where the chamber transducer was not available.

The normal operating procedure for the combustor is as follows. The fuel valve is opened. Fuel enters the unit via venturi action caused by the incoming air, so no fuel flows initially when the valve is opened. The spark plug is then activated using a 120 Hz. ignition coil. The starting air is then pulsed using bursts of approximately 1-2 sec. duration. The starting air is a small, high pressure, axially oriented jet that simultaneously entrains ambient air and forces it into the chamber and creates local suction at the fuel venturi causing it to flow as well. When the unit first starts, the starting air is run continuously for approximately 1 second while the spark plug is turned off. Finally, the starting air is turned off and the pulse combustor runs self-aspirated until the fuel valve is closed. Successful starts can run for up to 15 seconds before the unit gets unacceptably hot. However, since parts of the fiber optic position sensor are plastic (including the fiber), test durations were typically under 4 seconds in duration. All data was collected digitally at a 50 kHz. sampling rate. The fuel used was gasoline. The fuel metering jet used was 0.039 in. in diameter.

III. Results

A. Reed Valve

A trace of the chamber pressure, p_{cc} and position sensor voltage (heretofore referred to as the fiber), V_{fiber} during self-sustained limit cycle operation is shown in Fig. 8. Pressure is plotted as an offset from ambient, p_a (i.e., gage or differential). Displacement is simply plotted as fiber voltage and is subtracted from the estimated value corresponding to the valve being fully closed. Approximately 24 cycles are shown in order give a sense of cycle-to-cycle variability. The operational frequency is 203 Hz as determined by power spectral density analyses of the chamber pressure, the fiber voltage, and the microphone signal. The mean chamber pressure is 3.8 psig, which is typical of design operation. This corresponds to approximately 4.6 lb_f of static thrust.

To view the cycle in detail, a phase-locked, ensemble average of 50 cycles was constructed. The phase-locking signal was the moment in each cycle when p_{cc} dropped below 11 psia. The resulting single cycle traces are shown in Fig. 9. Several interesting features are notable in this figure: 1) the open period appears considerably shorter than the closed period; 2) the valve appears to bounce off the seat after initially slamming shut; 3) the valve does not begin to open until the chamber pressure is well below ambient; 4) the valve is almost completely closed by the time the chamber pressure has risen to ambient pressure. The general implication of these observations is that valve opening

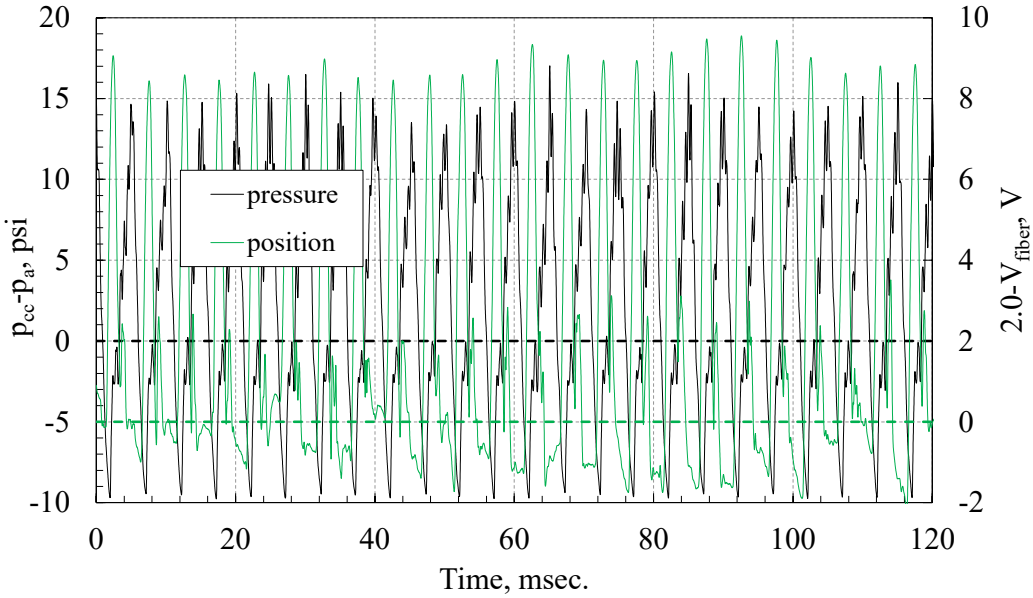

Fig. 8 Traces of chamber pressure and valve position vs. time over 24 cycles of the self-aspirating, reed-valved pulse combustor.

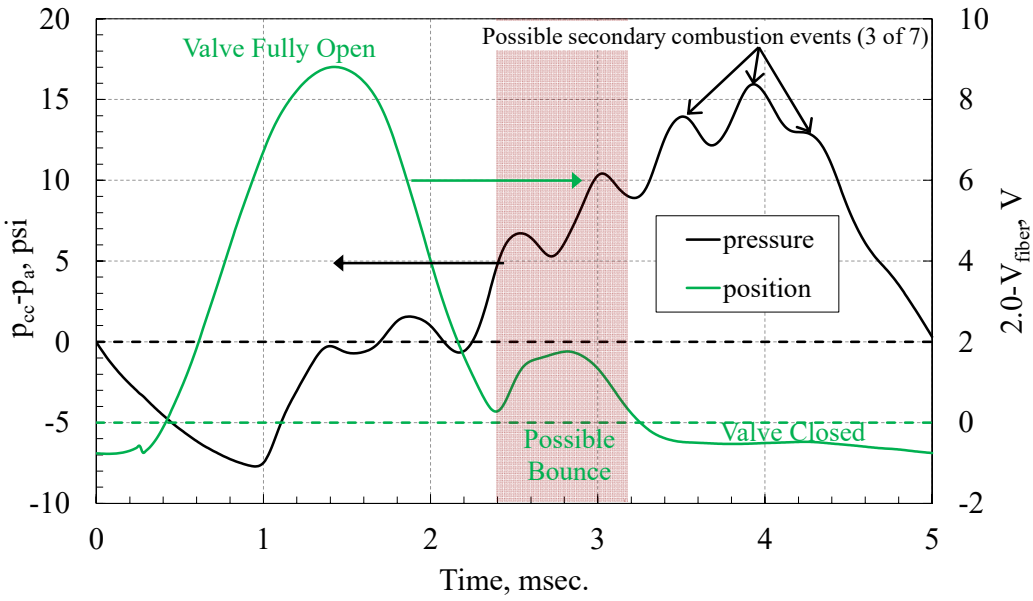

Fig. 9 50-cycle phase-locked, ensemble-averaged traces of chamber pressure and valve position vs. time over one cycle of the self-aspirating, reed-valved pulse combustor

is dominated by pressure forces on the valve, but closing is driven by the highly non-linear reed valve spring. When the reed valve is fully open (bottom of Fig. 5) the rim of the valve stop becomes a pivot point for the portion of the reed that protrudes into the flow. This has the effect of increasing the effective spring constant immensely. The reed is quickly decelerated and subsequently 'flung' back in the direction of closure.

Two frames from a high speed video (20 kHz frame rate) looking down the inlet during operation are shown in Fig. 10. Figure 10a is thought to be from the intake portion of the cycle. Fuel droplets are visible, along with 2 small jets of fuel coming from the injection holes at approximately the 4 o'clock and 8 o'clock positions. Figure 10b is thought to be from the period shortly after the combustion event has commenced in the chamber. A flash of some sort is visible indicating that hot gas has been driven upstream from the combustion chamber and into the inlet. The two frames of Fig. 10 are seen every cycle. The flash is likely a confirmation of either the valve bouncing as indicated in Fig. 9, or the valve not being completely closed when the chamber pressure rises above ambient. Both would cause hot gas backflow and potential ignition of some of the fuel and air in the inlet. It is noted however that the events described in Fig.10 a and b could not be synced to the chamber pressure or probe movement. Hence, it is not known with certainty which portion of the cycle the respective images represent.

Also seen in Fig. 9 are approximately 7 high frequency oscillations (≈2300 Hz.) in the chamber pressure during the combustion event (i.e., as the pressure rises). Their cause is unknown, and they are not believed to have a bearing on the valve operation. Their frequency is on the order of the pressure transducer standoff tube acoustic resonance frequency; however, the observation that they are present only during the combustion event makes this an unlikely cause. They are noted here as a point of interest and to gain appreciation for the complexities of this flow field.

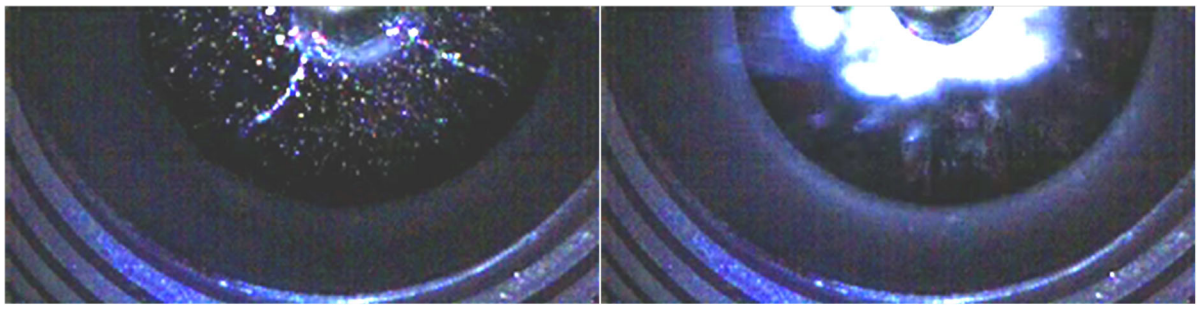

(a) **(b)**

Fig. 10 High speed video frames of the pulse combustor inlet showing (a) intake period; (b) initial combustion period during reed valve operation

B. Poppet Valve

None of the parametric testing of the poppet valve yielded self-aspirated operation. The starting process described earlier would commence, and a weak thermo-acoustic process of some sort would typically commence. The sparking unit could be turned off, but the forced starting air would have to flow continuously for the process to be maintained. The valve was designed with 4 different spring stiffness options and 3 damper thickness and hardness combinations. The results to be shown represent the best of the parametric testing. Additionally, it was found that removing the diverter shown in Fig. 4 improved operation (such as it was), so all results utilize this configuration. All the springs chosen for the poppet valve placed a static preload on the poppet in the closed position. This meant that the forced starting air had to be driven at a higher pressure in order to force flow into the pulse combustor. Figure 11 shows traces of p_{cc} and V_{fiber} as functions of time for 24 cycles of limit cycle operation. This is to be compared to Fig. 8. The operational frequency is 292 Hz. The mean chamber pressure is 0.0 psig, indicating no developed thrust. The pressure oscillations are seen to be very small. The poppet appears to barely close at best. It is also seen that the phase relationship between the valve opening and the pressure oscillations is completely different. This is shown clearly in the 50 cycle ensemble average of Fig. 12, which compares with Fig. 9. Figure 12 also shows two frames from a high speed video of the valve motion during operation. The frames represent the maximum opening and degree of close over the course of one cycle. Although not shown in this paper, the position sensor was tested on one of the other 9 poppets comprising the complete valve system. The phase and amplitude results were nearly the same.

C. Additional testing

Since the poppet valve did show a weak resonance at a frequency above the value that the pulse combustor is tuned for (200-220 Hz.), a series of tests were conducted with different tailpipe lengths to see if the valve and pulse combustor could be better tuned. This was accomplished using several inexpensive chamber and tailpipe assemblies purchased commercially for the hobby scale DynaJet pulsejet. These are dimensionally identical to the present pulse combustor, but are fabricated from thin-walled stainless steel. As such, they cannot be instrumented with a chamber pressure transducer. As a crude substitute, an external microphone was mounted outside the combustor, approximately 2 ft. from the tailpipe exit and 90 degrees from the axis of symmetry. The microphone signal can be processed to measure operational frequency. The rms value of the signal serves as a measure of combustion chamber pressure fluctuations, and therefore the degree of resonant operation. Four different lengths were tested as shown in Fig. 13. It is noted that simply changing the tailpipe length is a crude method to use for altering the operating frequency. The diameter of the tailpipe, the dimensions of combustion chamber, and the chemical and fluid time scales all couple to form the operational frequency. Since a length change was easy to accommodate however, it was deemed a worthwhile test. Figure 13 also shows one combustor tailpipe that is longer than the original. It was fabricated by adding length to one of the commercial pulsejet tailpipes. Testing a longer tailpipe is counter-intuitive to the idea of

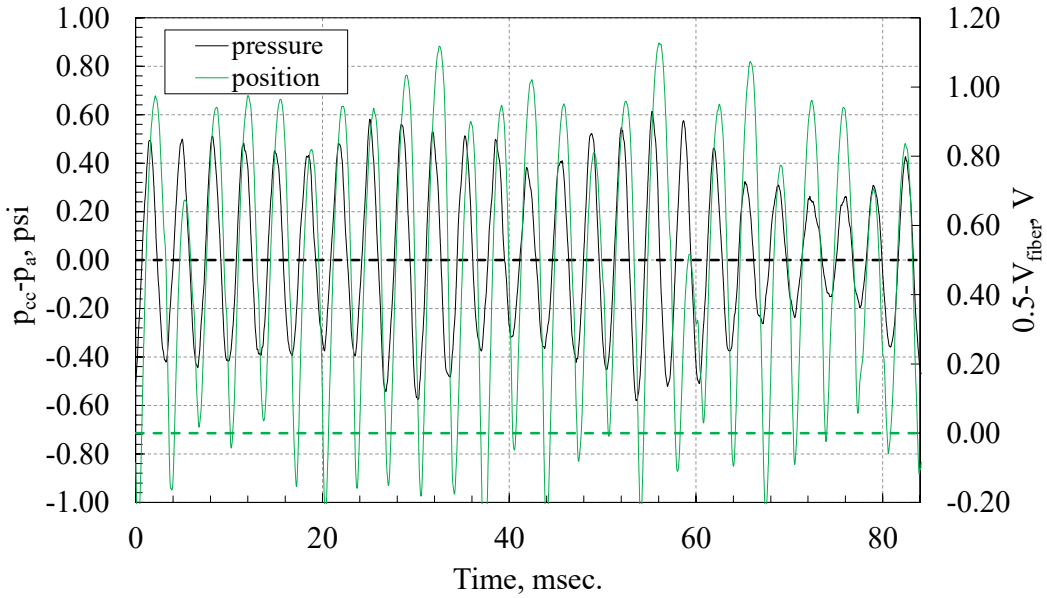

Fig. 11 Traces of chamber pressure and valve position vs. time over 24 cycles of the forced-aspiration, poppet-valved pulse combustor.

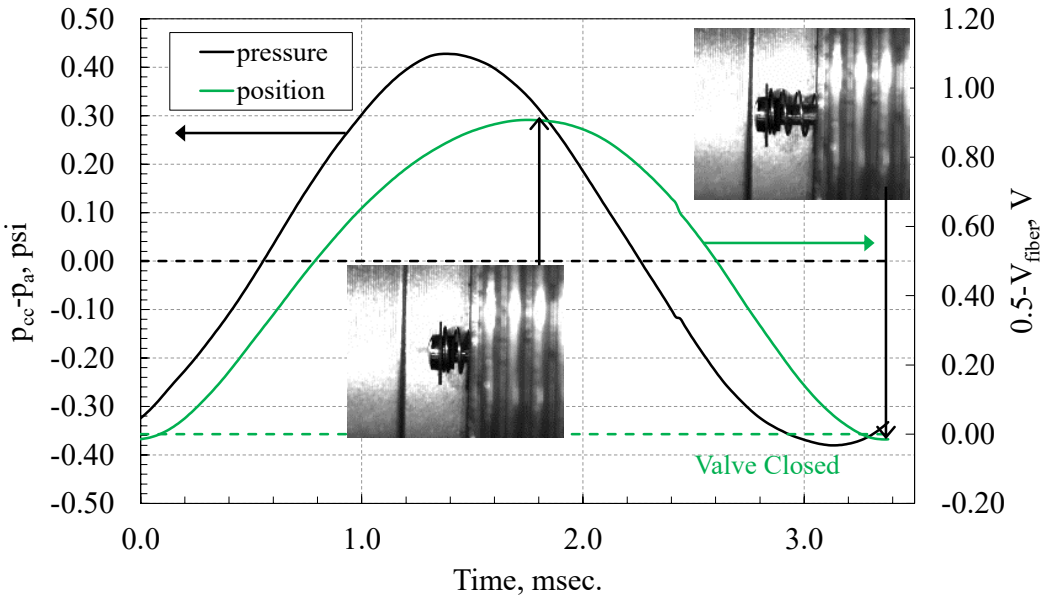

Fig. 12 50-cycle phase-locked, ensemble-averaged traces of chamber pressure and valve position vs. time over one cycle of the forced-aspiration, poppet-valved pulse combustor

raising the operating frequency. The test was conducted because the particular unit was available from previous testing campaigns, and because anecdotal evidence suggests that lower operating frequencies are less sensitive to valve dynamics and chemical kinetics [10]. Tests were conducted with both the reed and poppet valves.

Results of the testing are listed in Table 1. All frequencies were verified in the power spectra of both the position sensor and the microphone. The microphone rms signal strength is shown in dB. This is calculated as follows.

$$dB = 20Log\left(\frac{rms_{operational}}{rms_{ambient}}\right) \quad (1)$$

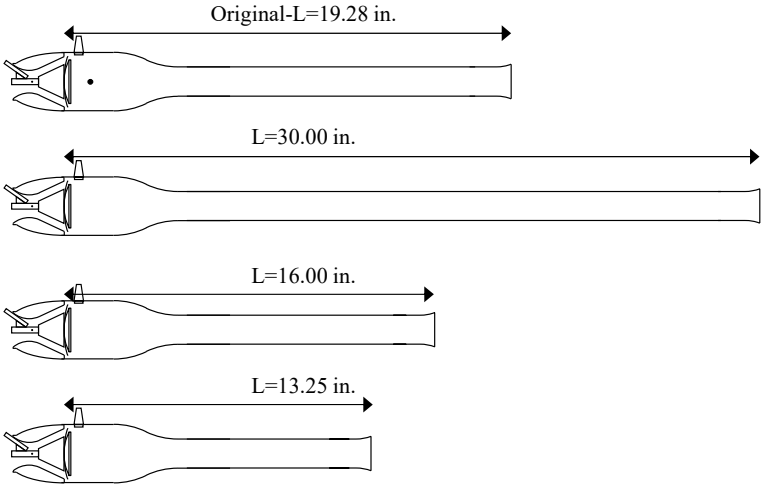

Fig. 13 Pulse combustor length variations

Here, $rms_{operational}$ is the rms of the signal during pulse combustor operation, and $rms_{ambient}$ is the rms of the signal in the ambient laboratory environment. It is noted that the ambient environment includes a quite loud ventilation fan, which also runs during operation.

Shortening the tailpipe yielded even poorer performance than the original length. Additionally, the acoustic signal frequency of the system went down for the poppet valve (counter to expectations) and up for the reed valve. The valve position data was not studied since there was no reason to do so.

The longest tailpipe configuration proved the most interesting. Testing with the reed valve produced self-aspirated operation, with a microphone signal strength just slightly below the original tailpipe length. A power spectral analysis of both the microphone and valve position signal yielded two dominant frequencies, one below, and one above that of the original tailpipe length.

Testing with the poppet valve did not produce self-aspiration. However, it did produce the strongest microphone signal strength observed for the poppet valve. Oddly, the dominant frequency was nearly the same for all the tailpipe lengths tested with the poppet outside of the original tailpipe.

Traces of the poppet and reed valve positions over several cycles of the long tailpipe configuration are shown in Fig. 14. The dual frequency behavior of the reed valve is evident in the observation that there are two maxima per cycle. The poppet valve motion is notable for the apparent bouncing associated with its closing. This could also be caused by minor lateral vibrations of the poppet within the sleeve.

Table 1 Performance of various length pulse combustors

	Frequency Hz.	Microphone dB	Self-Aspirating (yes/no)
Reed	202	36.5	Yes
Poppet	296	6.7	No
L=19.28 in			
Reed	140/268	35.9	Yes
Poppet	197	15.3	No
L=30.00 in			
Reed	330	3.4	No
Poppet	199	3.0	No
L=16.00 in			
Reed	336	0.8	No
Poppet	205	2.7	No
L=13.25 in.			

IV. Computational Modeling

To further aid in diagnosing the reasons for the vastly different reed and poppet valve performance, simplified mathematical models were developed to roughly approximate the observed valve motion as a function of time, and the forcing of the chamber pressure. The models were then implemented in a validated computational fluid dynamic (CFD) model of the pulse combustor [6, 8] in order to obtain the combustor pressure response to the valve motion (i.e., to provide coupling). The CFD model will be described briefly below, followed by the valve models.

A. CFD Model

A previously successful effort to simulate the current experiment is used in here. It is an in-house code which solves the axisymmetric, unsteady, Reynolds averaged Navier-Stokes equations for a multi-species, thermally perfect, chemically reacting gas. The turbulence model used in the calculations is the Spalart-Allmaras one-equation model. The liquid gasoline of the experiment is replaced with gaseous Jet-A in the code and is injected closer to the chamber since no time is needed for atomization and vaporization. The computational domain includes the interior of the pulse combustor and some free space downstream of the tailpipe exit plane so that the well-known vortex that is emitted each pulse can be captured. The outer surface of this free space is held at ambient pressure as a boundary condition. The pulse combustor inlet plane is maintained at constant total pressure, with the value being equal to the ambient pressure. Solutions are obtained on the NASA Advanced Supercomputer (NAS). Typical simulations have approximately 100,000 grid points, and require approximately 4.5 wall hours per cycle (using 15 processors), with 6-10 cycles required to achieve limit cycle operation.

The original simulation utilized a kind of sliding valve to approximate the reed valve. It is shown in Fig. 15. The motion of the valve was prescribed. It opened at a user specified rate when the chamber pressure dropped below atmospheric. It closed at a similar rate when the chamber pressure rose above ambient. The prescribed opening/closing rate was such that the valve moved to its open or closed position over 15% of the cycle time. This may be thought of as a very crude (i.e., notional) active valve strategy with feedback control. However, the mechanical means required to achieve the motion and rates was not considered. The original simulation reasonably matched the experimental reed valve pulse combustor in terms of thrust, chamber pressure amplitude and average value, mass flow rate, and frequency. Specifically, the average chamber gage pressure of the simulation was 33% below the experiment, the mass flow rate matched exactly, and the operational frequency was 22% above the experiment. An example limit-cycle solution at a moment in time from [8] is shown as contours of temperature in Fig. 16. It illustrates the entirety of the computational space, as well as the fluidic complexity of the solution.

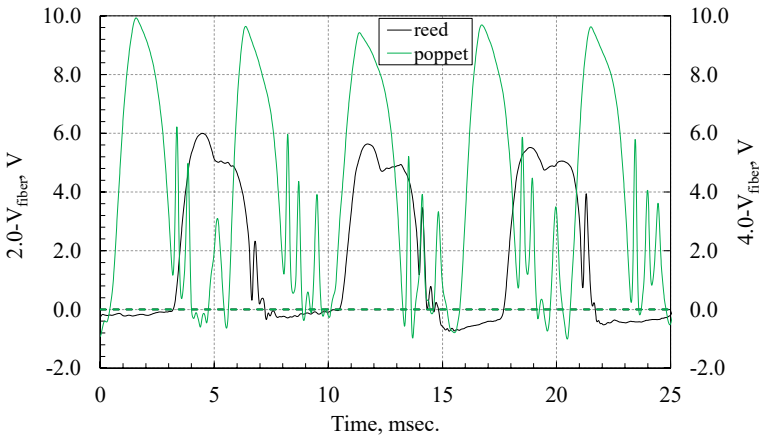

Fig. 14 Poppet and reed valve position over several cycles of the 30 in. tailpipe configuration

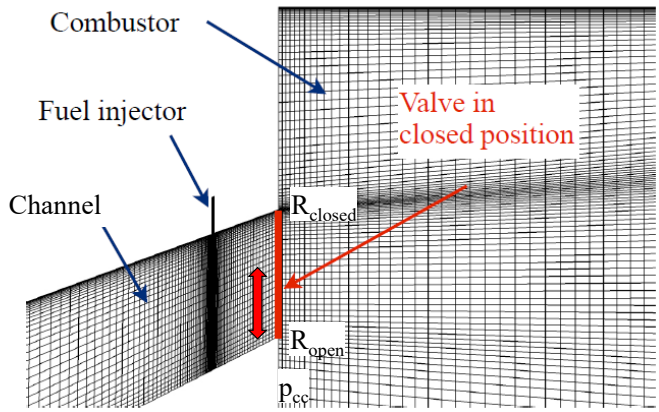

Fig. 15 Notional slider valve used in CFD simulation of the experimental pulse combustor

With reference to Fig. 15, the slider valve open area relative to the inlet channel area is closely approximated by the following equation.

$$\frac{A_{vs}}{A_{ch}} = \frac{R_{closed} - R_{vs}}{R_{closed} - R_{open}} \tag{2}$$

Here, R_{vs} is the radial location of the outer tip of the slider valve. The valve thus slides down (i.e. radially inward) to open.

The experiment used liquid fuel that was introduced through jets via a venturi system as shown in Fig. 2. During the fill portion of the cycle, the pressure at the fuel jet location drops below ambient, and fuel is drawn through the jets since the fuel manifold is held at ambient pressure. In the CFD model, a gaseous injector as shown in Fig. 15 is used. The injector mass flow rate is driven by a user specified manifold pressure. The injector is turned on or off each cycle based on the valve opening or closing. The fuel manifold pressure was tuned to best match experimental results. It was observed that a fuel-rich environment was necessary to achieve any kind of self-aspirated operation, which is consistent with experimental results. The reason for this is thought to be related to the poor mixing and distribution properties of the fuel injection system more than any chemical kinetics associated with rich combustion. For example, the Ref. [8] work showed that simply changing the location of the fuel injector from the wall to mid-channel could yield the same performance with less fuel consumed.

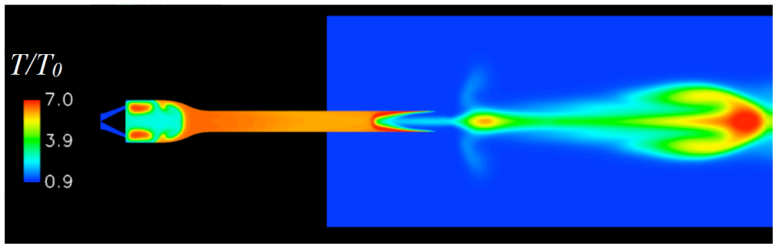

Fig. 16 Contours of normalized temperature showing the CFD solution of the present experiment at a moment in time using the active, feedback-controlled slider valve [8].

B. Reed Valve Model

The actual physics of the reed valve motion is complex since it is highly non-linear. For this work, it is approximated as a poppet valve that is identical in dimension and mass to the current poppet valve, but with linear travel distance that is approximately the same as the 0.018 in. of the reed valve shown in Fig. 5. The governing equation set for velocity and displacement is that for a forced spring mass system with damping [9].

$$\frac{dv_v}{dt} = \frac{12g_c}{m}\{(p_a - p_{cc})A_p + F_s - fv_v\} \tag{3}$$

Here, v_v is the valve velocity in in/s, m is the mass of one poppet (or reed valve petal) in lb_m, g_c is the Newton constant in $lb_m \cdot ft/\ lb_f \cdot s^2$, f is a friction coefficient in $lb_f \cdot s/in$, F_s is the spring force in lb_f, and A_p is the area of one of the 10 poppets (i.e., reed valve petals) in in^2. In order to capture the non-linear flinging aspect of the reed valve, the spring force is divided into two regions.

$$F_s = \begin{matrix} -kx_v; x_v \le 0.17\ in. \\ -100kx_v + 99k(0.17); x_v > 0.17\ in. \end{matrix} \tag{4}$$

The spring constant k is 2 lb_f/in. The valve displacement, x_v is in inches. The values for m, f, and A_p are respectively, 0.00042 lb_m, 0.0015 $lb_f \cdot s/in.$, and 0.1 in^2. Some of these values were measured. Others were chosen to match dynamic data. The valve velocity and position are related by definition.

$$\frac{dx_v}{dt} = v_v \tag{5}$$

Equations 3 and 5 can be integrated numerically if p_{cc} is known as a function of time. Provision must be made for when the valve fully closes. Figures 8 and 9 indicate that a bounce occurs on impact. Modeling such a scenario is beyond the scope of this work. Instead, the valve is simply prevented from moving beyond the fully closed position, and once it is closed, as long as the forces are pushing it leftward in Fig. 5, the velocity is set to zero. This is easily accomplished through logical statements embedded in the numerical integration. It is equivalent to mandating an inelastic collision when the valve slams shut.

The response of the reed valve model when subjected to the chamber pressure profile of Fig. 9 is shown in Fig. 17. For comparison, the measured fiber-optic probe displacement profile is also shown. The two profiles cannot be directly compared since the probe can't be calibrated, and is non-linear. Still, it is evident that the opening, closing, and peak positions are temporally aligned.

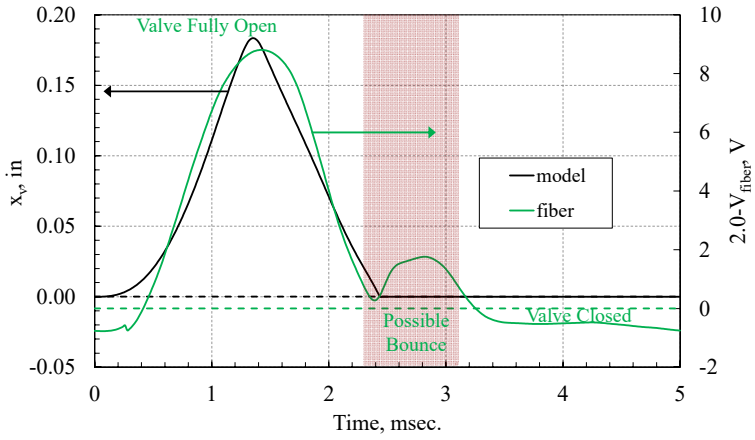

Fig. 17 Modeled and measured reed valve response to the Fig. 9 chamber pressure profile.

The open reed valve area relative to the channel area is linearly related to the displacement.

$$\frac{A_{vr}}{A_{ch}} = \frac{4x_v}{d_{ch}} \tag{6}$$

Here, d_{ch} is the diameter of one of the 10 channels comprising the inlet and is equal to 0.36 in. When the valve is at a displacement of 0.09 in., Eq. 6 takes on a value of 1. At peak displacement the value is 2. However, the flow path from channel to chamber is a tortuous one. As such, in the context of mapping this open area on to the slider valve open area (which has a relatively straight forward flow path), an effective reed valve area is used. This is equivalent to prescribing a variable discharge coefficient to the reed valve, and a constant discharge coefficient of 1.0 to the slider valve.

$$\begin{gathered}\frac{A_{vs}}{A_{ch}} = 0.65\frac{A_{vr}}{A_{ch}}; \frac{A_{vr}}{A_{ch}} \le 1 \\ \frac{A_{vs}}{A_{ch}} = 0.65 + \frac{0.35}{0.5}\left(\frac{A_{vr}}{A_{ch}} - 1\right); 1 \le \frac{A_{vr}}{A_{ch}} \le 1.5 \\ \frac{A_{vs}}{A_{ch}} = 1.0; \frac{A_{vr}}{A_{ch}} \ge 1.5\end{gathered} \tag{7}$$

Equation 2 can then be rearranged to obtain the slider valve tip position.

$$R_{vs} = R_{closed} - \frac{A_{vs}}{A_{ch}}\left(R_{closed} - R_{open}\right) \tag{8}$$

Equations 3-8 are then implemented in the CFD model. At a moment in time, the CFD model has the p_{cc} and x_v (and therefore R_{vs}). Equations 3-5 are then advanced one time step to obtain the next value for x_v, which is mapped to a new value of R_{vs}. The code then advances one time step to obtain the next p_{cc}. This repeats until a limit cycle is reached. In the experiment, p_{cc} is measured at the position shown in Fig. 2. In the code, it is measured at the position shown in Fig. 15 ($0.77 \cdot R_{open}$). Simulation results indicate that the temporal values at the two locations are nearly indistinguishable. Because the CFD model yields higher operating frequencies than the experiment, it is noted here that a smaller value of 0.00025 lb_m was used for the spring mass.

1. *Coupled CFD Passive Reed Valve Model Results*

The simulation was initiated with a computational domain state from the Ref. [8] simulation. The initial state was temporally just after the original slider valve had closed. A new limit cycle was reached in approximately 7 cycles.

A plot of the chamber pressure and valve position over the course of one cycle is shown in Fig. 18. The similarity to experiment (Fig. 9) is remarkable. The average chamber gage pressure is 30% below the experiment (the average of the absolute pressure is just 6% below the experiment), the mass flow rate was 13% below the experiment, and the

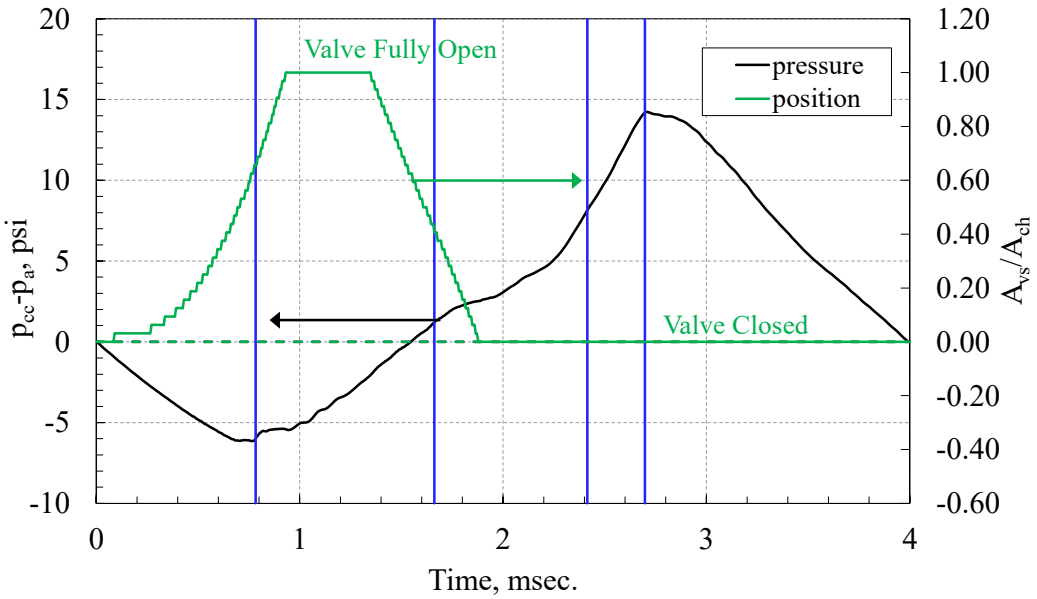

Fig. 18 Traces of chamber pressure and valve position vs. time over one cycle of the CFD simulation with reed valve model after reaching limit-cycle operation.

operational frequency was 23% above the experiment. Also shown in the figure are 4 vertical blue lines representing instants of time during valve opening, valve closing, combustion initiation, and near combustion completion. The chamber flowfield during these times is illustrated with contours of temperature and fuel mass fraction in Fig. 19. It appears from Figs. 18 and 19 that the CFD model with the simple reed valve sub-model has successfully captured the fundamental mechanical and fluid dynamic physics of this passively valved system.

C. Poppet Valve Model

The poppet valve model is the same as the reed valve model with two exceptions. First, the spring valve force is changed to the following.

$$F_s = -kx_v; k = \ 1.5 \ \mathrm{lb}_f/in \tag{9}$$

Second, the poppet valve is prevented from moving beyond 0.1 in. from the closed position. Thus, in a mirror image of the inelastic closing response described above, once it reaches x_v=0.1 in., as long as the forces are pushing it rightward in Fig. 5, the velocity is set to zero.

It was not possible to validate this model against operational data as was done for the reed valve (see Fig. 16). Since the poppet valved configuration could not operate in a self-aspirated mode, the starting air was always forcing air into the system. This forcing is not built into the model and was impossible to characterize with the existing instrumentation. Furthermore, since the operational pressure oscillations were so weak, it was not clear that they were the result of a cycle anything like the one described in Fig. 1. It is possible that the measured pressure oscillations were more localized and did not have the same phase relationship with the pressure near the valve which controls its opening and closing. Nevertheless, a comparison was attempted between the valve model and the measurements. The results are shown in Fig. 20 in the same manner as Fig. 17. The forcing chamber pressure profile is that of Fig. 12. However, the ambient pressure was raised by 0.18 psi over the measured value in order to simulate the effects of the starting air jet. This value was selected because it resulted in the poppet valve model just barely closing fully (i.e. no dwell time in the closed position) which was consistent with the position sensor results. The shapes of the two Fig. 19 profiles are similar, but it is clear that there is a significant phase difference. One possible reason for this has already been discussed. There are many other possibilities, but all are speculative. Moreover, none could be readily modeled in the framework of the present simulation. As such, and because this computational effort is diagnostic in nature, the poppet model presented was considered sufficient. It is noted in passing that Eq. 9 does not include a preload on the spring as was described earlier. Adding it resulted in a required forcing pressure from the start air that was deemed unrealistically high. Furthermore, the resulting valve movement was much less than that seen in the high speed video of Fig. 12.

1. *Coupled CFD Passive Poppet Valve Model Results*

As with the reed valve, the coupled simulation was initiated with a the end state of a previous simulation. In this case it was that of the passive reed valve simulation presented above. The simulation showed a steady decline in chamber pressure oscillation amplitude, average mass flow rate, and cycles averaged chamber gage pressure (i.e. thrust) over the entire approximately 8 cycles that it has executed as of this publication. The chamber pressure and valve position over approximately 7 of these cycles are shown in Fig. 21. The cycle averaged chamber gage pressure during the seventh cycle is 73% below the experiment and still dropping. The operational frequency has dropped from 242 Hz. to 220 Hz. The cycle is clearly trending toward either substantially reduced limit cycle performance, or complete failure. Note that the valve completes closure when the chamber pressure is well above ambient. This results in backflow of hot gas into the inlet channel which reduces the mass flow rate and the pressure rise (due to lack of confinement). The reduced peak pressure further reduces mass flow rate since the subsequent expansion is also weakened, which creates less suction during the inflow period. The chamber flowfield during the four instants shown in blue in Fig. 21 are presented as contours of temperature and fuel mass fraction in Fig. 22. The backflow just described is evident.

These results, particularly in contrast to the reed valve simulation, suggests that the limited travel and damping valve stop associated with the poppet valve were responsible for the steady cycle decay (and possible failure) of the poppet valve simulation.

It is interesting to note that the operational frequency of the simulation (240-220 Hz.) was well below the experimentally measured frequency (292 Hz.). This observation adds plausibility to the previously stated suggestion that the oscillations observed in the experiment were caused by something other than the classical pulse combustor cycle described in Fig. 1.

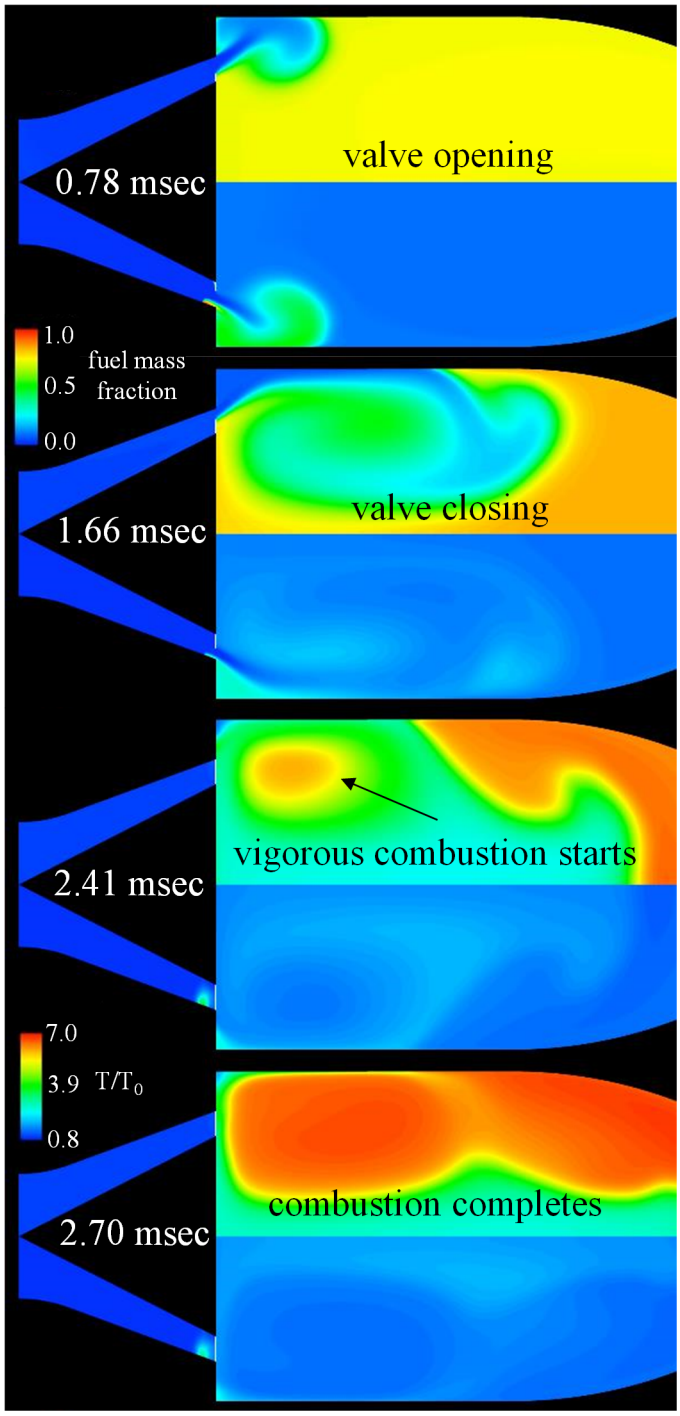

Fig. 19 Contours of temperature (upper half) and fuel mass fraction (lower half) during the four instants of time shown in Fig. 18 of the CFD reed valved model limit cycle.

V. Discussion

The passive poppet valve simulation showed a slow, but continuous decline in chamber pressure oscillation amplitude and other performance indicators, but it did run for multiple cycles. The experiment could not run at all without forcing. And as discussed, it is not obvious that the oscillations observed were evidence of a proper pulse combustor cycle. The reason for these different behaviors was likely that the simulation was initiated from a previously successful limit cycle, whereas the experiment has to be started from what amounts to a perturbation. The cycle has to build-up in a kind of bootstrapping process from a small pulse. Liquid fueled pulse

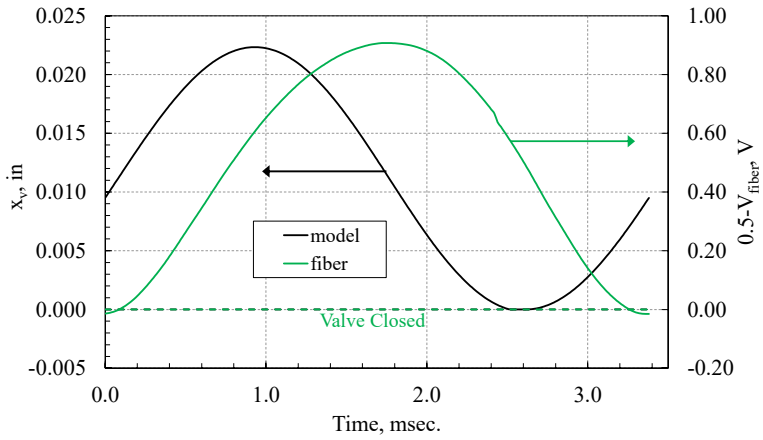

Fig. 20 Modeled and measured poppet valve response to the Fig. 12 chamber pressure profile.

combustors are known to be difficult to start, and the poor poppet valve performance during this starting process may have been just enough to prevent the necessary bootstrapping.

It is also worth noting that the simulation may have persisted longer than it should have because fuel flow did not decrease as the air mass flow rate went down. Fuel flow in the experiment is governed by a venturi system which in turn is regulated by the air mass flow rate. If the air mass flow rate is reduced by the limited travel of the poppet, this could reduce the fuel flow to such a degree that the cycle fails. Even under the best of circumstances, venturi-fed pulse combustors are not throttleable. They operate at a single set point. In contrast, the simulation uses a pressure-driven, actively valved fuel delivery system. A reduction in mass flow rate did not lead to a reduction in fuel flow rate in the simulation because the user defined fuel manifold pressure was not reduced from the value used in the reed valve simulation. Time constraints did not allow an exploration of the effects of reducing this manifold pressure in accordance with the air flow rate.

Regardless of the above stated possibilities for simulation and experimental differences, it is evident that the poppet valve described herein does not perform as well as the reed valve. Modifications to the design such as lengthening the valve stem to increase linear travel distance, or replacing the damper with a non-linear Belleville disc spring to provide the same rapid closure as the reed valve could be considered. However, both modifications add mass to the poppet and will affect dynamic response. Furthermore, even if they did succeed in making the valve work properly, the resulting motion and stresses would likely be very similar to the short-lived reed valve that it was meant to replace.

The results from this investigation show clearly that a very specific valve motion is necessary for high performance pulse combustion at high frequency, and that passive valve designs which can deliver the requisite motion and survive many cycles are a significant challenge. A more promising approach may be to consider active designs. Doing so would likely require an inlet flow path substantially different than that of Fig. 2. The 10 diverging holes comprising

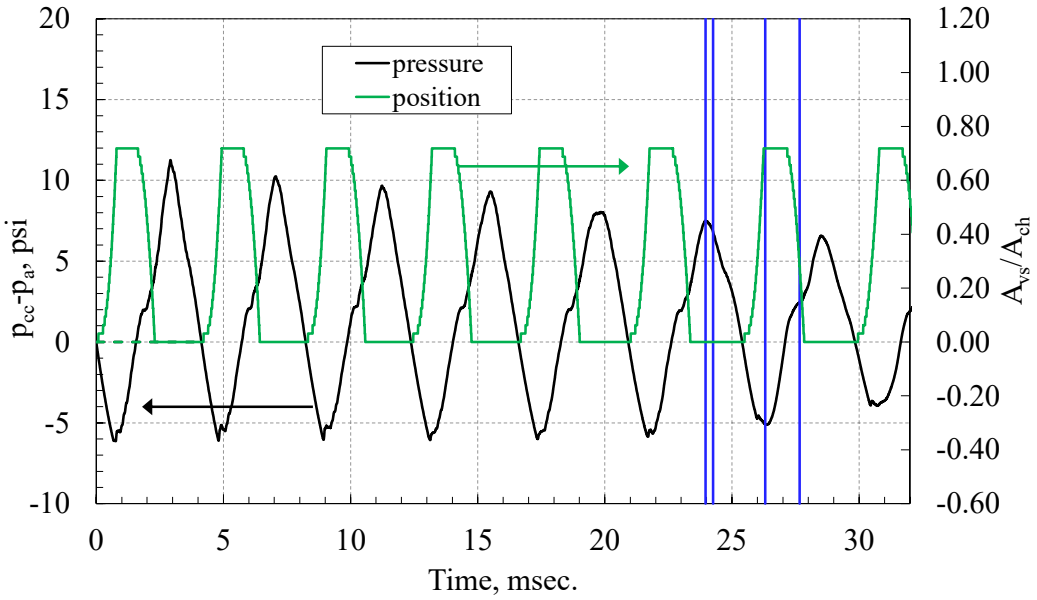

Fig. 21 Traces of chamber pressure and valve position vs. time over seven cycles of the CFD simulation with poppet valve model after initializing with the end state of the simulation with the reed valve model.

that inlet make any kind of actively actuated motion nearly impossible. Inlet flow path optimization is readily achievable with the CFD capabilities described in this work. And active valve concepts that can provide the needed opening and closing rates in a low stress manner seem quite possible.

VI. Conclusion

The motion of two types of passive valves operating in a small scale, liquid-fueled pulse combustor was investigated experimentally. One was a reed style valve and the other was a poppet valve. Both used the same valve head and inlet channel. Valve position and combustion chamber pressure were measured simultaneously using an in-house fabricated optical position probe. The reed valve configuration operated in a self-aspirated mode, generating significant pressure gain. The poppet valve configuration could not operate without forced air, did not generate pressure gain, and developed very weak oscillations. Subsequent testing of the poppet valve in combustors of multiple lengths yielded worse performance for lengths shorter than the original, and only a slight improvement for lengths longer than the original. Self-sustained, self-aspirated operation was never achieved. Comparison of the respective valve motions indicated that the non-linearity and significant travel of the reed valve are essential for self-aspiration. Dynamic models for the motion of each valve were implemented in a computational fluid dynamic (CFD) simulation of the pulse combustor and verified that the unique reed valve motion is necessary for successful operation. The results highlight the challenges associated with long-lived, high-performance, passive valve design in high frequency pulse combustors. They further highlight the need for active valve actuation with feedback control.

Acknowledgements

The authors would like to thank Tom Barkis for designing and assembling the electronics of the optical position probe. They are grateful too for his assistance in configuring and running the data acquisition equipment. They also wish to thank John Ramsey and Lawrence Kren for the design and fabrication of the poppet valve. And finally, they are grateful to Yolanda Hicks for provision of, and assistance with, the high-speed video camera.

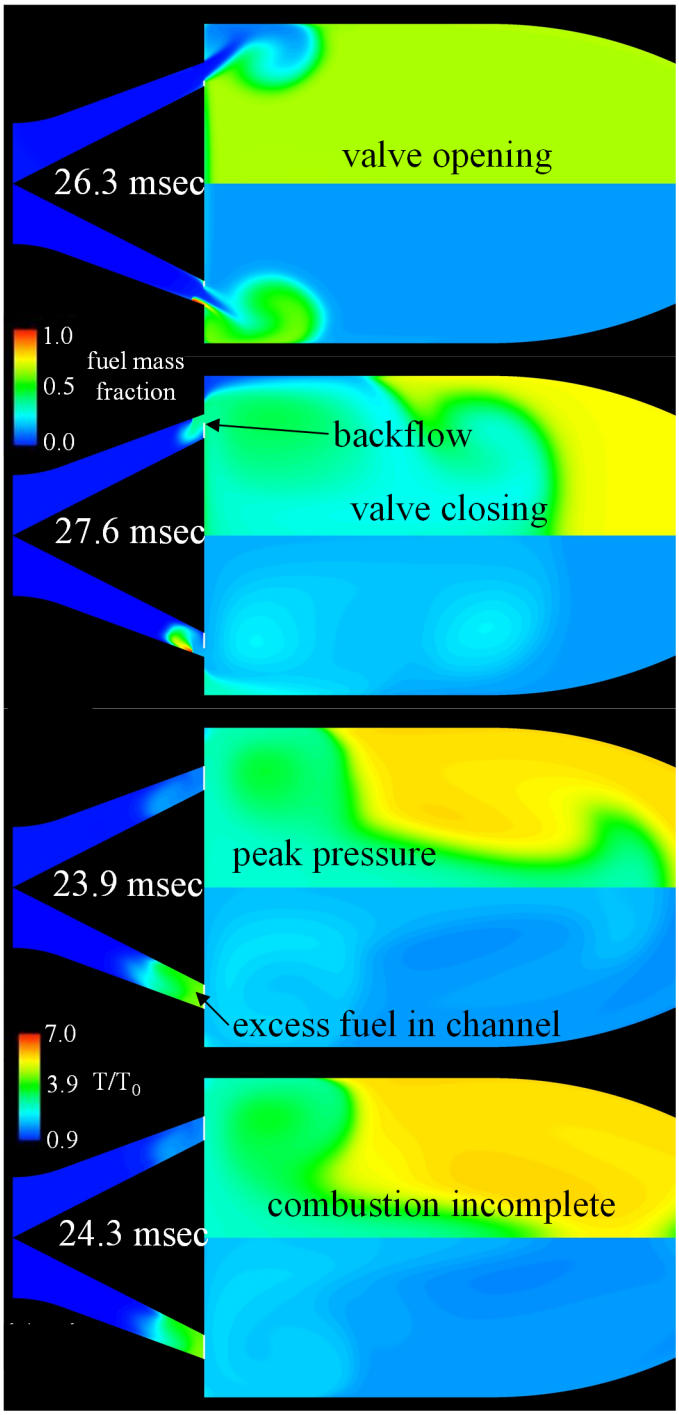

Fig. 22 Contours of temperature during four instants of time in the sixth and seventh cycles of the CFD poppet valved simulation.

References

[1] Paxson, D. E., Wilson, J., and Dougherty, K., "Unsteady Ejector Performance: An Experimental Investigation Using a Pulsejet Driver," AIAA 2002-3915, July, 2002.

[2] Lisanti, J. C. .,Zhu, X., Guiberti, T. F., Roberts, W. L., "Active Valve Resonant Pulse Combustor for Pressure Gain Combustion Applications," *AIAA Journal of Propulsion and Power*, Vol. 38, No. 2, 2022, pp. 171-180.

[3] Anand, V., Jodele, J., Prisell, E., Lyrsell, E., Gutmark, E., "Dynamic Features of Internal and External Flowfields of Pulsejet Engines," *AIAA Journal*, Vol. 58, No. 10, 2020, pp. 4204-4211.

[4] Paxson, D.E. and Dougherty, K., "Ejector Enhanced Pulsejet Based Pressure Gain Combustors: An Old Idea With a New Twist," AIAA 2005-4216, July 2005.

[5] Paxson, D.E., Dougherty, K.T., "Operability of an Ejector Enhanced Pulse Combustor in a Gas Turbine Environment," AIAA 2008-119, January, 2008.

[6] Yungster, S., Paxson, D.E., Perkins, H.D., "Numerical Investigation of Shrouded Ejector-Enhanced Pulse Combustor Performance at High Pressure," *AIAA Journal of Propulsion and Power*, Vol. 33, No. 1, 2017, pp. 29-42.

[7] Kentfield, J.A.C, Nonsteady, One-Dimensional, Internal, Compressible Flows, Oxford University Press, 1993, p. 193.

[8] Yungster, S., Paxson, D. E., Perkins, H. D., "Computational Study of Pulsejet-Driven Pressure Gain Combustors at High-Pressure," AIAA 2013-3709, July, 2013.

[9] Geng, T., Zheng, F., Kuznetsov, A.V., Roberts, W.L., Paxson, D.E., et al, "Comparison Between Numerically Simulated and Experimentally Measured Flowfield Quantities Behind a Pulsejet, Flow," *Turbulence and Combustion*, Vol. 84, No. 4, pp. 653-667, May 2010.

[10] Litke, P. J., Paxson, D. E., Schauer, F. R., Bradley, R. P., Hoke, J. L., "Assessment of the Performance of a Pulsejet and Comparison with a Pulsed-Detonation Engine," AIAA 2005-0228, January, 2005.